Supplementary Information for

Anticorrelation Between Local Photoluminescence and Photocurrent Suggests Variability in Contact to Active Layer in Perovskite Solar Cells

Giles E. Eperon, David Moerman and David S. Ginger*

Department of Chemistry, University of Washington, Seattle, WA 98105, USA

*Email: dginger@uw.edu

Supplementary Data

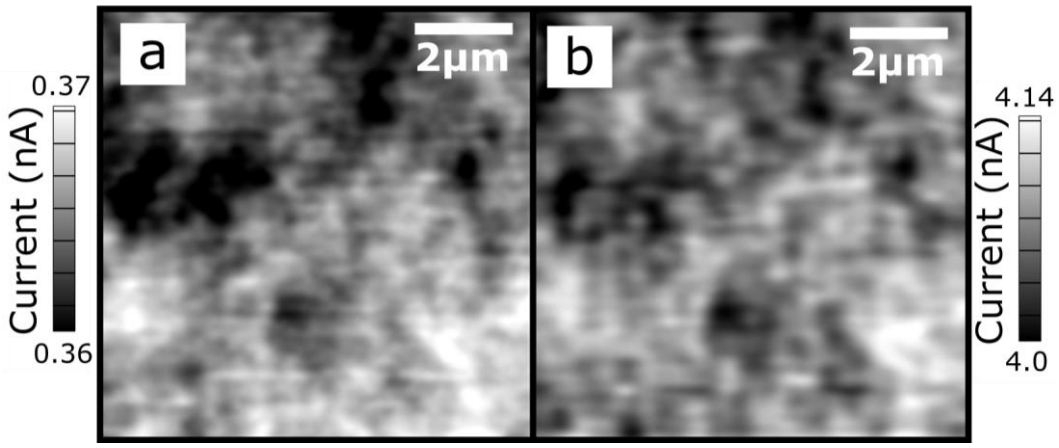

Fig. S1. LBIC images of the same area on a device, taken at a) ~2 suns (2200W/m^2) and b) ~22 suns (22000W/m^2) laser intensities.

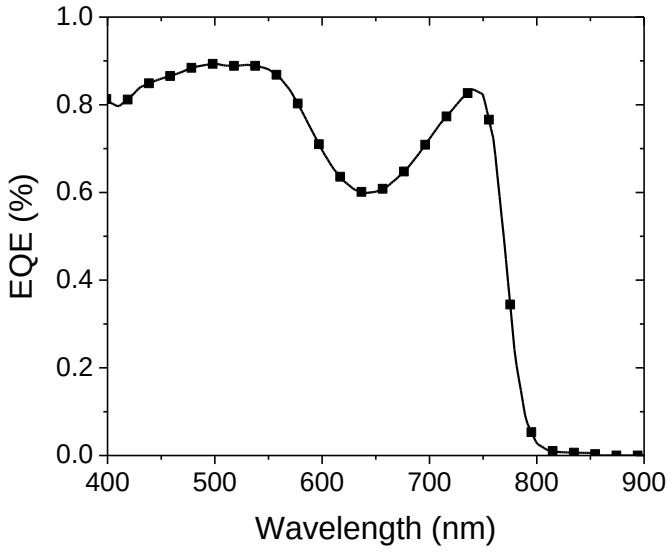

Fig S2. External quantum efficiency spectrum for a typical device used in this work. Integration of the product of this spectrum with the AM1.5 spectrum gives a short-circuit current of 19.7mAcm^{-2}.

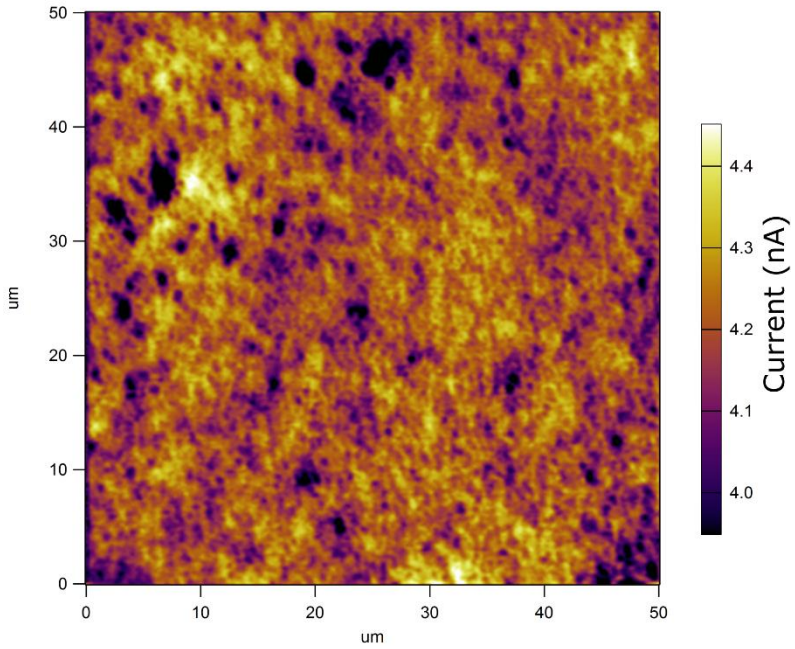

Fig. S3. Larger area LBIC map showing similar heterogeneity over larger area.

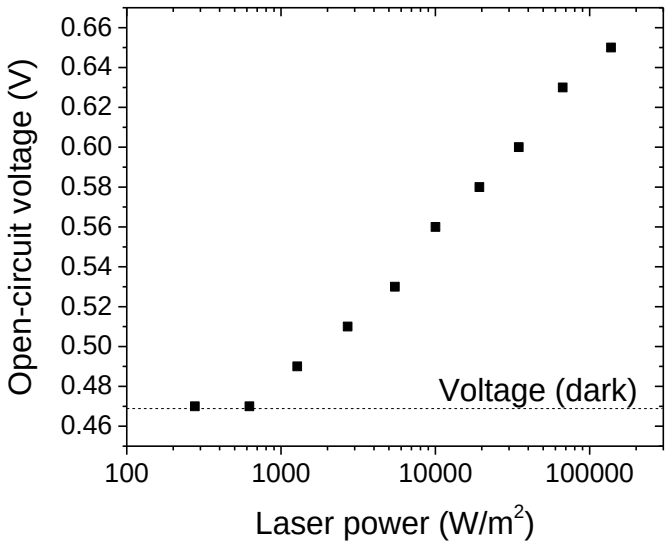

Fig S4. Voltage measured for cell as a function of laser illumination intensity, showing that at the power normally used (10000W/m^2) we are within the logarithmic relation regime. This cell had an open-circuit voltage of 1.05V under full area AM1.5 100mWcm^{-2} illumination.

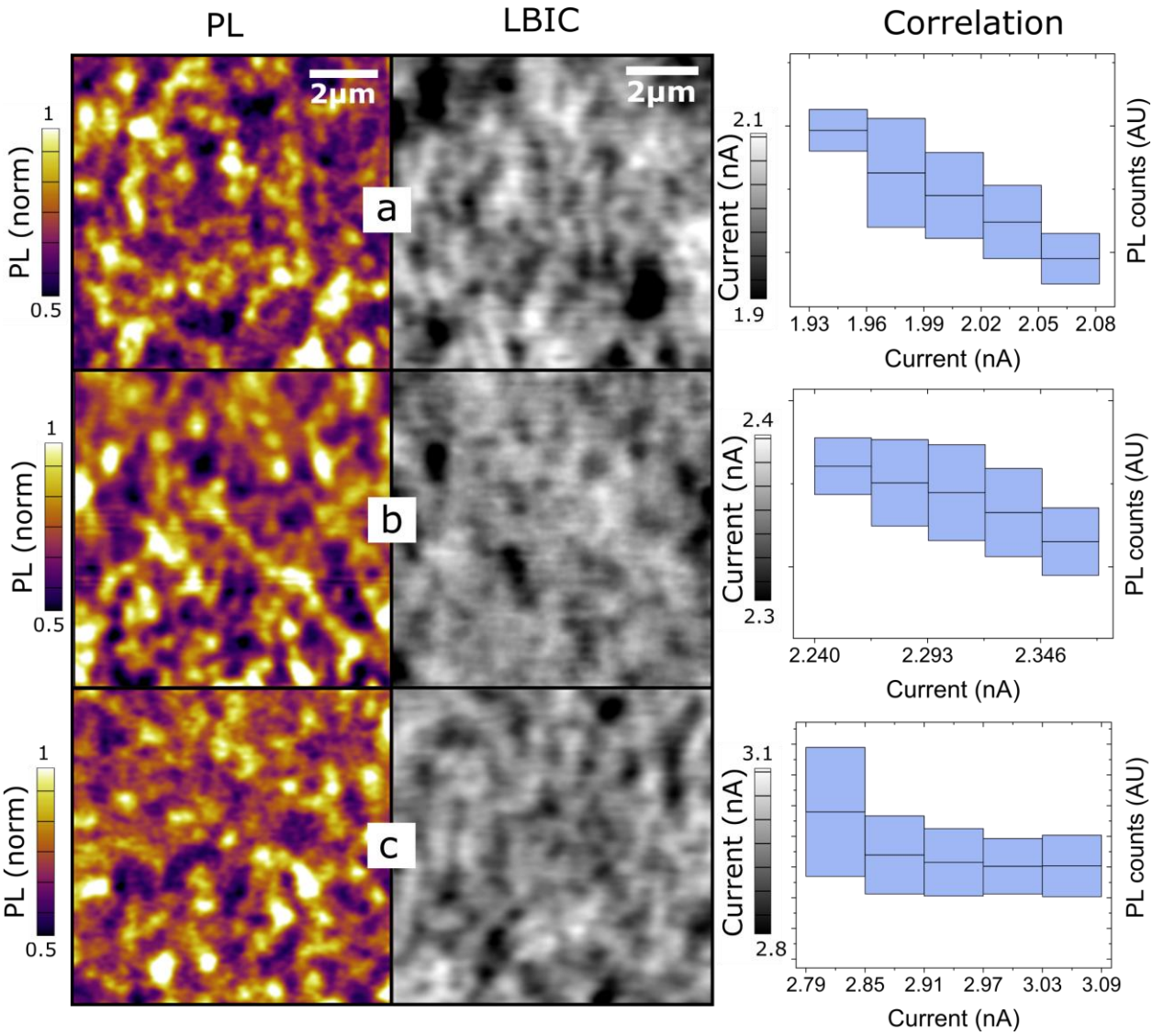

Fig S5. a,b,c) Additional regions of separate devices showing visual anticorrelation between PL maps (left) and LBIC maps (centre). The PL intensity as a function of binned current is shown on the right. Films illuminated with pulsed laser at 1200-2200mW/cm^{-2}.

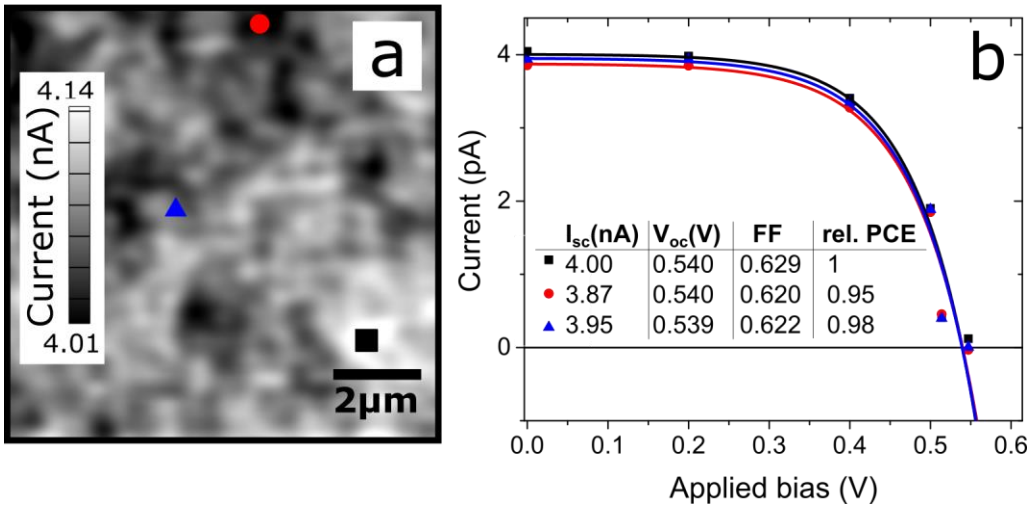

Fig S6. Current-voltage curves extracted from regions of high(black square), medium (blue triangle) and low (red circle) current, and extracted PV parameters. Varying bias was applied to the sample, measuring LBIC maps at each voltage and fitting JV curves to the current values at the three points using the diode equation. Solid lines are the fitted curves, data points are shown by the solid points.

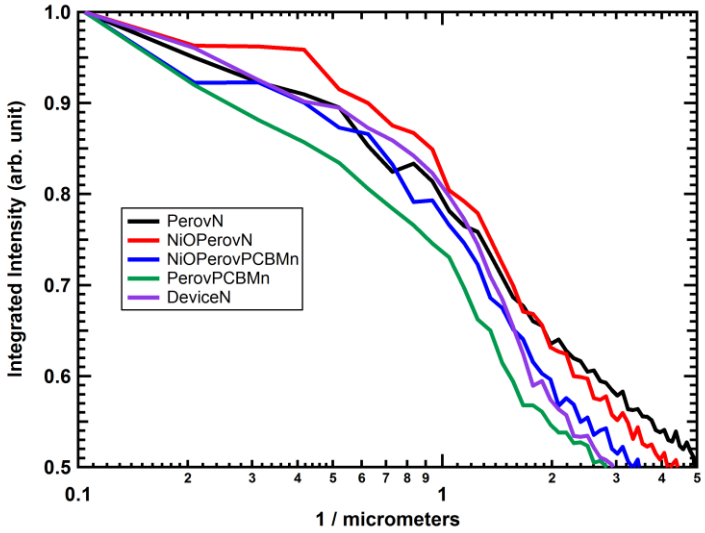

Fig. S7. Radially integrated FFT of PL maps taken from various configuration devices in Fig 4.

Device no.	Coefficient of variation
1	*0.189*
2	*0.203*
3	*0.166*
4	*0.106*
5	*0.134*
6	*0.237*
Average	***0.172±0.047***

Table ST1: Coefficient of variation for multiple PL maps taken on full device structures.

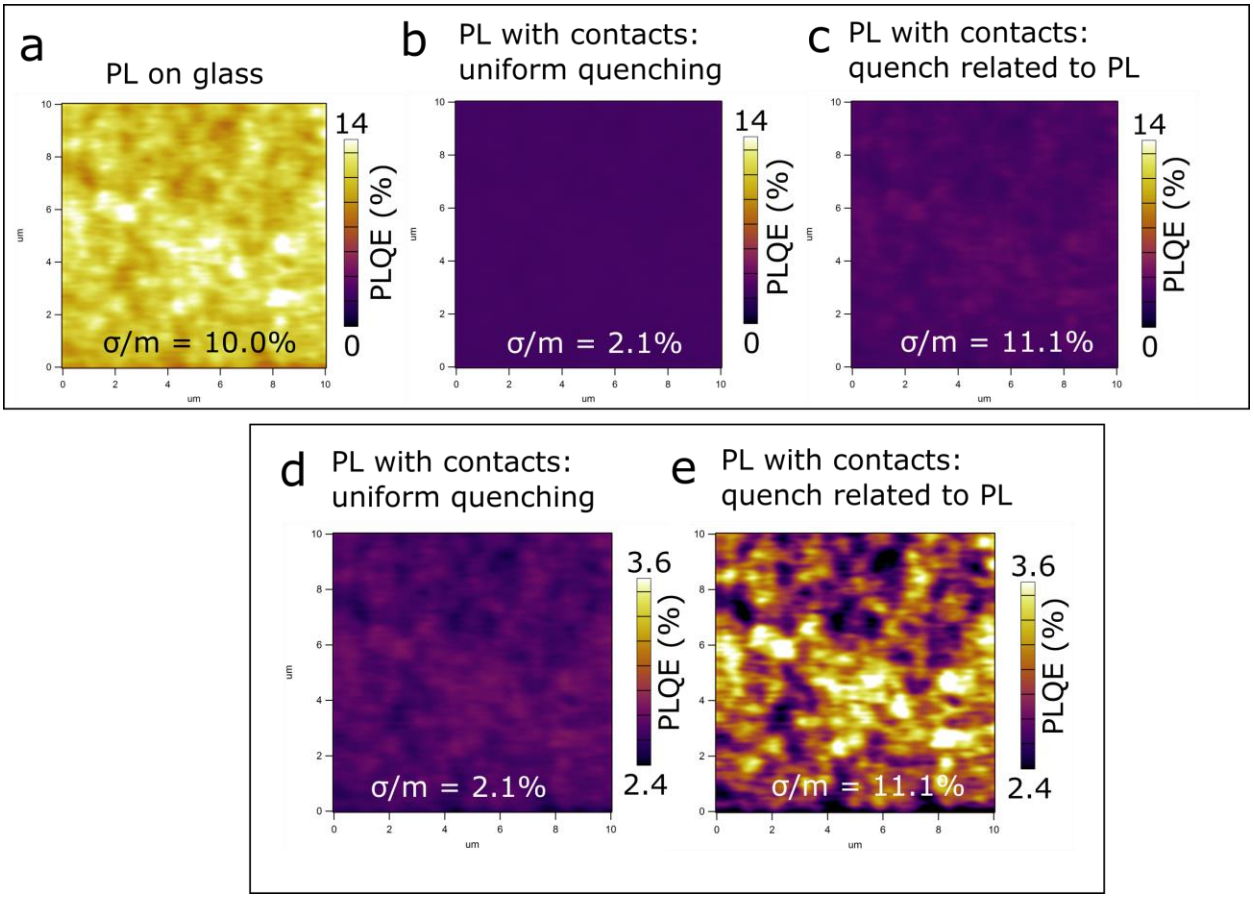

Fig. S8. Predicted PL maps and coefficient of variation calculations when contacts quench uniformly or when the quenching rate is linearly related to the non-radiative recombination rate (effectively determining PL brightness). a) PL map on glass scaled to give reasonable PLQE values (~10%). b) PL and coefficient of variation expected if quenching rate was uniform across the sample, plotted on same scale. c) PL and coefficient of variation expected if quenching rate is linearly related to non-radiative recombination rate (bright regions have lower non-radiative rate, and we test the case where they also have less effective quenching), plotted on the same scale. d), e) the same two quenched cases plotted on a finer scale to allow better visual comparison.

Model details: *We set the radiative recombination rate to be constant across the film, and the non-radiative recombination rate was determined from the film on glass to give approximately reasonable PLQE, using the relation PLQE = $k_r/(k_r+k_{nr})$, with k_r and k_{nr} being radiative and non-radiative rates respectively. When contacts are introduced we add another term for the quenching rate (k_q) so the equation becomes PLQE = $k_r/(k_r+k_{nr} + k_q)$. We then set the value for k_q as constant for the uniform quenching case and as a multiplicative factor of k_{nr} for the PL-related case. In both cases we adjust the constant / multiplier until PLQE values are reasonable for that measured (~2%).*

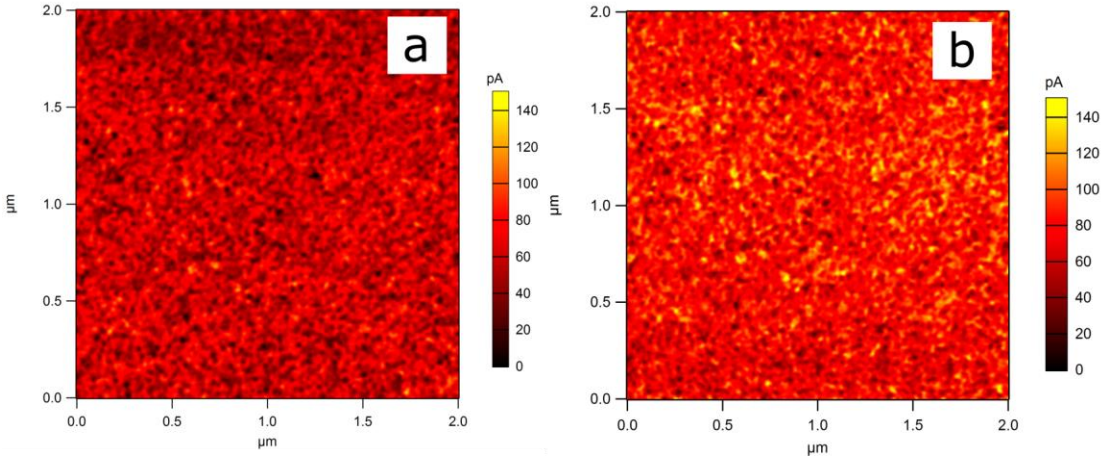

Fig S9. Conductive AFM scans at a) -0.2V and b) +0.2V sample bias on ITO/NiO showing homogeneity of nickel oxide contact layer on the length scales over which heterogeneity is present in devices. Note that the current in a) was in the opposite direction to b).

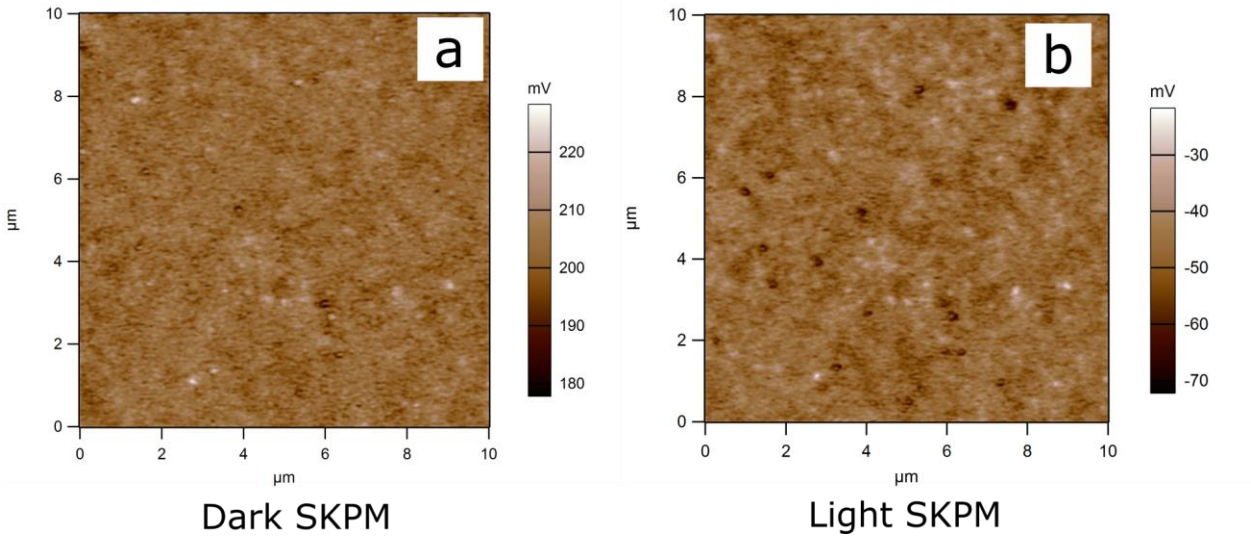

Fig. S10. Scanning Kelvin Probe microscopy images of the same area on an ITO/NiO/perovskite film in the dark (a) and under illumination (b) showing negligible heterogeneity in the work function. Work function is measured relative to the Pt-coated tip.

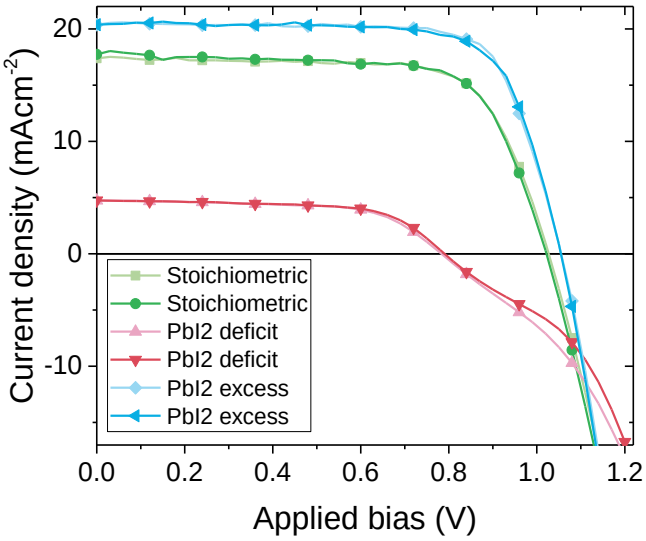

Fig. S11. Current-voltage characteristics measured under 100mWcm^{-2} AM1.5 illumination for the best performing devices made with the three stoichiometries – PbI_2 excess, deficit and stoichiometric.

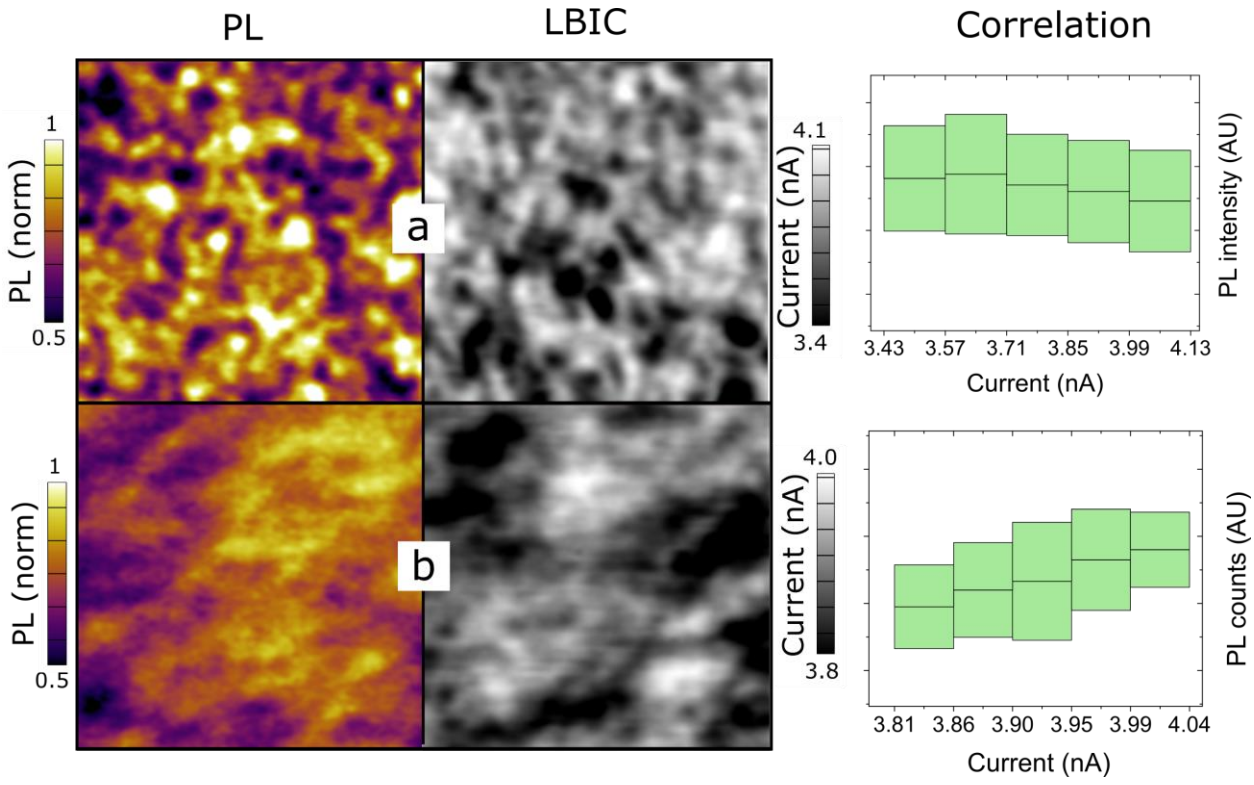

Fig. S12. More regions of PL, LBIC and plots showing correlation for devices made with stoichiometric MAI:PbI_2 ratio.

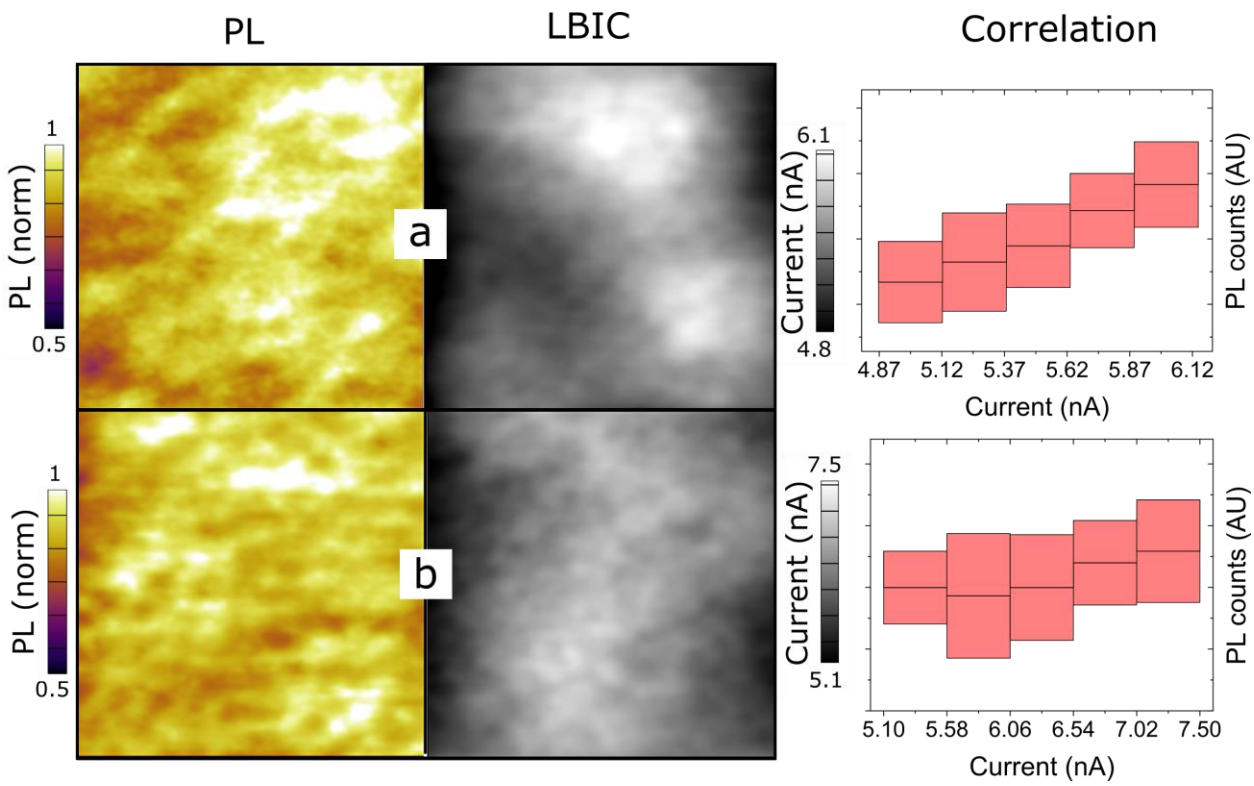

Fig. S13. More regions of PL, LBIC and plots showing correlation for devices made with a deficit of PbI_2. We note that higher power laser intensity (~8800mW/cm^{-2}) was needed to attain contrast in the PL.

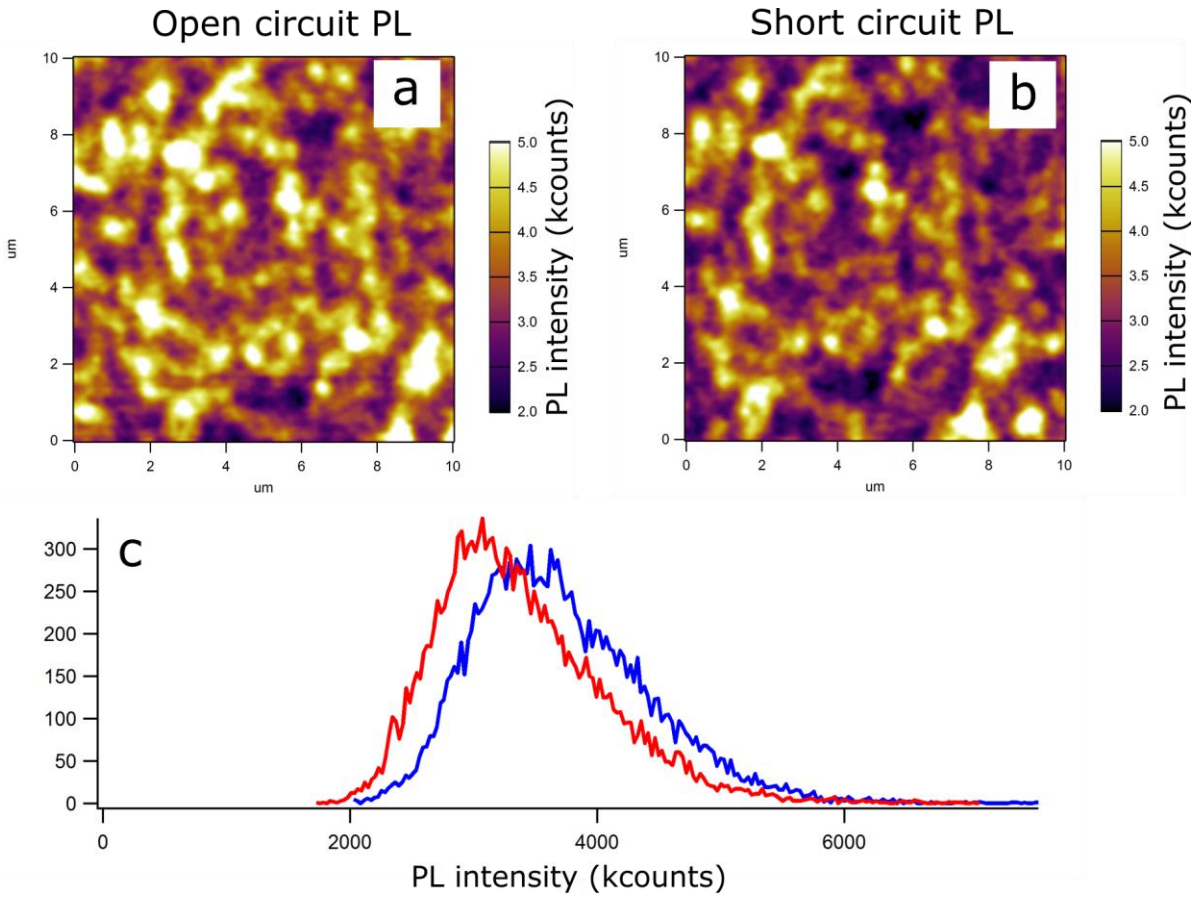

Fig. S14. Comparison of PL measured at open circuit (a) and short circuit (b) showing small degree of quenching. c) Comparison of the two PL distributions on a histogram. red = short circuit, blue = open circuit.

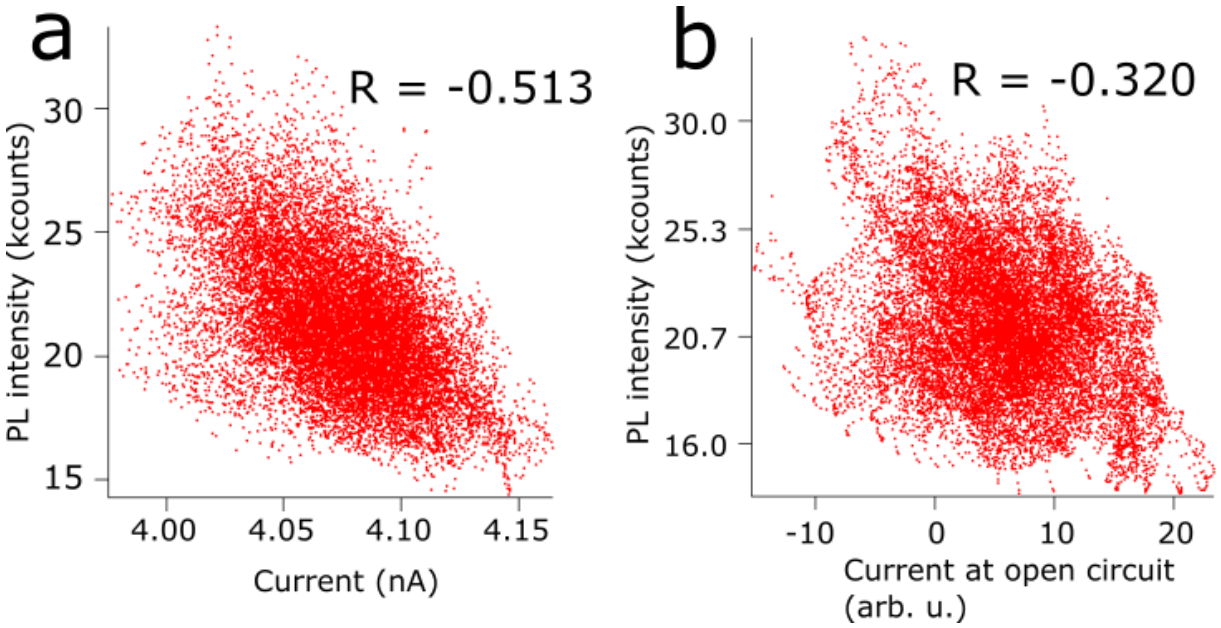

Fig. S15. Determination of correlation coefficients for PL vs LBIC and LBIV maps. The same data as used to generate box plots in Fig 3 is plotted in full here, and Pearson correlation coefficients (R) determined for each plot. a) shows PL plotted against LBIC and b) PL against current at open circuit, as used to extract relative voltage. The negative R values confirm significant anticorrelations. We note that the R values are generated by assuming a linear correlation, which may not hold here – based on current evidence we are unsure of the form of the expected relation, and experimental noise does not allow us to extract a form with confidence from fitting this data. However, the anticorrelation is clearly confirmed.

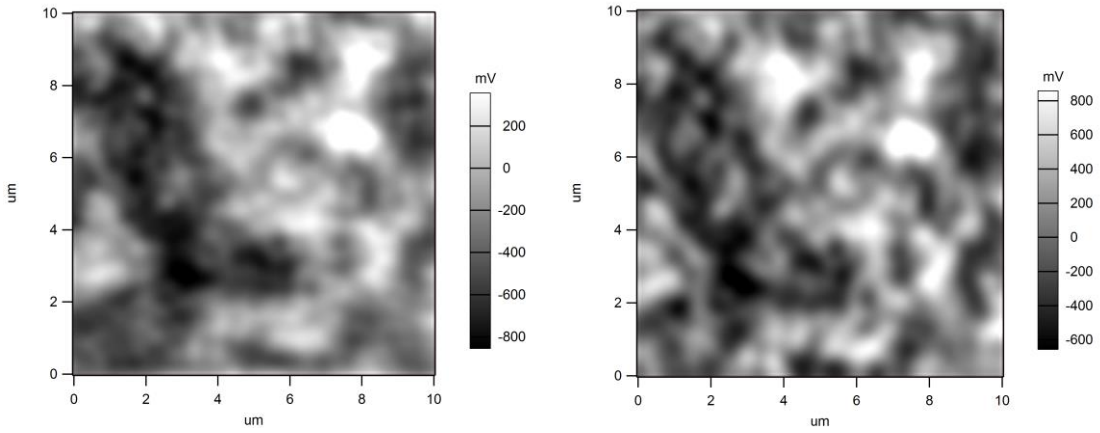

Fig. S16. Subsequent current scans taken at open-circuit voltage (0.574V for this cell) scanning up (left) and down (right), indicating that there is little change that is dependent upon scan direction. Each scan takes approximately 8 minutes.